Pergamon

NanoStructured Materials, Vol. 8, No. 2, pp. 179-189, 1997
Elsevier Science Ltd

0965-9773/97 $17.00 + .00

PII S0965-9773(97)00001-9

STRUCTURAL CHARACTERIZATION AND OPTICAL PROPERTIES OF NANOMETER-SIZED SnO_2 CAPPED BY STEARIC ACID

Xiaochun Wu*, Bingsuo Zou*, Jiren Xu*, Baolong Yu†, Guoqing Tang†, Guilan Zhang†, Wenju Chen†

*Institute of Physics, Chinese Academy of Sciences, Beijing, 100080, P.R. China
†Institute of Modern Optics, Nankai University, Tianjin, 300071, P.R. China

(Accepted January 7, 1997)

Abstract—*Structure and optical properties of nanometer-sized SnO_2 capped by a layer of stearic acid are investigated using TEM, XRD, ESR, UV-visible absorption spectrum, photoluminescence spectra, IR absorption spectra and Z-scan techniques. It is found that such capped SnO_2 samples display new optical properties, which will enlarge their applications in nonlinear optics. The relationship between structure and optical properties of the SnO_2 nanoparticles is also discussed.*

1. INTRODUCTION

From the viewpoints of both theoretical research and potential applications, nanoparticles have recently attracted great attention due to their unique structures and properties (1). On the one hand, with decreasing particle size, the electronic states of nanoparticles become discrete from continuous energy bands in bulk and the lowest exciton energy level blue-shifts. This is the so-called "quantum size effect" (2). Therefore, the study of the transition between their electronic levels has very important theoretical significance for understanding the transformation of matter from the macroscopic to microscopic state. On the other hand, the enhanced nonlinear optical responses of nanoparticles observed experimentally (3), making nanoparticles an attractive nonlinear optical material, has stimulated further research.

For the past ten years the study of nanoparticles has made great progress (4). In order to enlarge the material realm and find new nonlinear optical materials, SnO_2 was chosen as the subject for this work, because bulk SnO_2 is an important semiconductor material and it also has relatively large nonresonant third-order nonlinear optical susceptibility among inorganic oxides (5). In order to study its optical properties, nanometer-sized SnO_2 capped with a layer of stearic acid was synthesized and characterized through a series of spectroscopic techniques.

2. EXPERIMENTAL

2.1 The Synthesis of Nanometer-sized SnO_2 Sample

Nanometer-sized SnO_2 samples were prepared by the microemulsion method. 10 ml of newly-made $SnCl_4$ aqueous solution was added to 100 ml of xylene containing 1×10^{-3} mol of stearic acid. The resulting mixture was stirred to form a microemulsion, then 20 ml of 0.1 M NaOH aqueous solution was added to the microemulsion to produce hydroxide under stirring. When the reaction was completed, the reaction product was extracted into the organic phase, because its surface was capped with a layer of stearic acid, and then the reaction system was allowed to stand still in order to separate the organic phase from the water phase. The water phase was discarded and the organic phase was refluxed 0.5 hr, then let stand at room temperature. The small amount of water on the bottom of the flask was discarded and the organic phase was washed with distilled water several times to further purify the reaction product. After purification, the organic phase was distilled to remove the residual water, then nanometer-sized SnO_2 organosol was formed. One part of SnO_2 organosol (sample 1) was used to carry out TEM, UV-vis absorption, fluorescence and Z-scan measurements. The other part of SnO_2 organosol was distilled to dryness at reduced pressures to obtain SnO_2 powder capped with stearic acids, which was divided into two parts. One is sample 2, and the other was heated at 400°C within a muffle to remove stearic acid (sample 3). The two powder samples were used to carry out XRD, FTIR, and ESR measurements.

The reaction schematic diagram is shown as follows:

$$\mathrm{SnCl_4\ aqueous\ solution} \xrightarrow[\text{organic solvent}]{\text{stearic acid}} \text{mixed solution} \xrightarrow[\text{dropping } OH^-]{\text{stirring}}$$

$$\mathrm{Sn(OH)_n^{m+}microemulsion} \xrightarrow[\text{washing}]{\text{refluxing}} \text{nanometer-sized } SnO_2 \text{ organosol}$$

$$\left\{\begin{array}{l}\text{part of } SnO_2 \text{ organosol as sample 1} \\ \text{nanometer-sized } SnO_2 \text{ (distilled to dryness)} \rightarrow \text{powder of} \left\{\begin{array}{l}\text{capped } SnO_2 \text{ powder as sample 2} \\ \text{(burn off surfactants) bare } SnO_2 \text{ powder as sample 3}\end{array}\right.\end{array}\right.$$

2.2 Measurement Instruments and Methods

The size of the nanoparticle organosol was measured through Philips EM-400 transmission electron microscopy (TEM). The average particle diameter was 7 nm. The XRD measurements were performed on Rigaku D/MAX-RA X-ray diffractometer using Cu K_α radiation source. Absorption and photoluminescence spectra were recorded on a Shimadzu UV-240 spectrophotometer and a RF-540 fluorimeter, respectively. IR absorption spectra were measured on Nicolet NX-240 FTIR spectrometer; wavenumber precision is 0.1 cm^{-1}. Mid-IR and far-IR measurements adopted KBr pelleting and nujol mull coating, respectively. The transmittances of two were normalized through computer and merged into one figure to output. ESR measurement was performed on Bruker 200D-SRC spectrometer. The magnetic field was calibrated with Mn^{2+} as a reference sample.

The Z-scan technique is a simple, sensitive, single beam method that uses the spatial beam distortion of laser pulse through a medium to measure the sign and magnitude of refractive variations. The details of the estimation procedure and theoretical background are well discussed in other literature (6 7). Generally speaking, the Z-scan curve for normalized transmittance versus Z, distance away from the focus, in defocusing materials ($n_{2<0}$) shows a prefocal maximum transmittance (peak) followed by a postfocal minimum transmittance (valley), while the curve in focusing materials gives rise to an opposite valley-peak configuration. The pure refractive nonlinearity shows a symmetrical Z-scan curve about Z=0, whereas the presence of an absorptive nonlinearity tends to distort the inversion symmetry of the curve. Absorptive saturation enhances the peak transmission and suppresses the valley, while multiphoton absorption produces the opposite effect. The closed aperture Z-scan experiment is sensitive to the refractive nonlinearity, while the open-aperture arrangement provides information about absorptive nonlinearity. Simultaneous adoption of two arrangements can help to determine the coefficients of both the absorptive and the refractive nonlinearity. Here, cw laser Z-scan measurement was carried with a cw Ar^+ laser as light source. Pulsed Z-scan was measured with 18-ns, 1.06 μm pulse from a Q-switched Nd:YGA laser, operating at a repetition rate of 1 Hz. The pulse energy is 30 μJ. The schematic representation of Z-scan measurement is shown as Figure 1. All experiments were performed at room temperature.

3. RESULTS AND DISCUSSION

3.1 XRD and ESR Measurements

Figure 2 is the X-ray diffraction spectra of the samples. According to JCPDS cards, Figure 2a belongs to monoclinic stearic acid whose main diffraction peaks lie at 2θ between 5° and 24°. The three main diffraction peak values of bulk SnO_2 in tetragonal rutile structure are located at 2θ of 27°, 33.9°. and 51.6°. In addition, between 60° to 70°, there still are a series of unidentified small

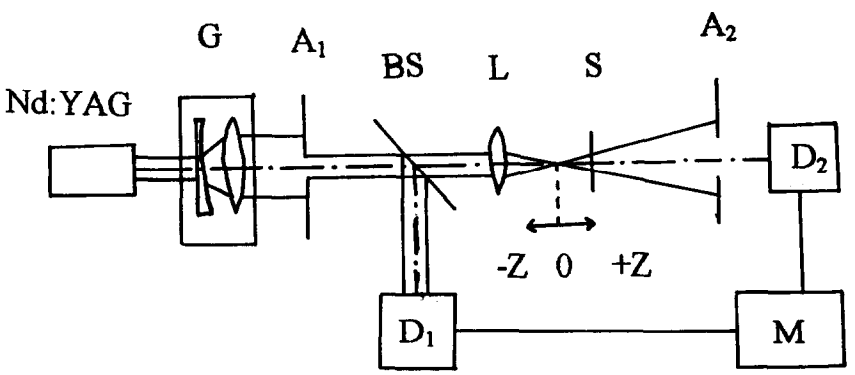

Figure 1. The schematic representation of pulse Z-scan measurements. G: beam extender; A_1, A_2: aperture; D_1, D_2: detector; L: lens; BS: beam splitter; S: sample; M: digital scope.

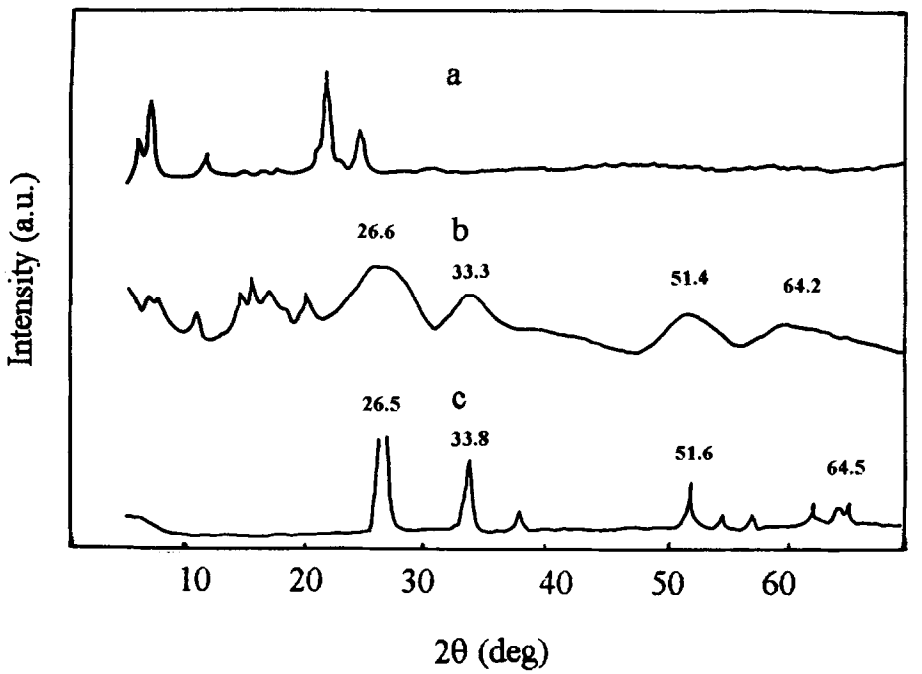

Figure 2. X-ray diffraction spectra of nanometer-sized SnO_2: (a) stearic acid; (b) sample 2; (c) sample 3.

diffraction peaks (8). Therefore, the main diffraction peaks of SnO_2 can be distinguished from those of stearic acid. In Figure 2b, the diffraction peaks below 24° belong to stearic acid, but the intensities of main diffraction peaks have changed a lot compared with those of Figure 2a, due to the possible crystal structure twist through the interaction with nanoparticles on the interface. The three main diffraction peaks of bulk SnO_2 are obviously broadened and a series of small diffraction peaks at high diffraction angle degrees are merged to a broad diffraction peak. According to the line-broadening of diffraction peaks to nanoparticles with good crystallinity, the size of crystallite could be calculated through the Scherrer formula. From the configuration of XRD spectrum, the as-prepared SnO_2 nanoparticles may mainly exist in the amorphous state and the size of the sample calculated from Scherrer formula may be much smaller than the actual size of the sample and is incorrect. This is justified by comparison of particle sizes byTEM measurement and calculation using the Scherrer formula. The crystallite diameter of sample 2 is 25 Å, according to the Scherrer formula, which has a large deviation from the 70 Å TEM result. The diffraction spectrum of sample 3 is similar to that of bulk SnO_2, as shown in Figure 2c. This indicates that under the conditions of high temperature and enough air, the capped surfactants are completely burned out and the nanoparticles continue to oxidize, grow, and become more crystalline.

From XRD analysis it could be concluded that the crystal structure of sample 2 is tetragonal rutile type, while there exists a large amount of amorphous structure on the interface of nanoparticles which has an interaction with capped surfactants.

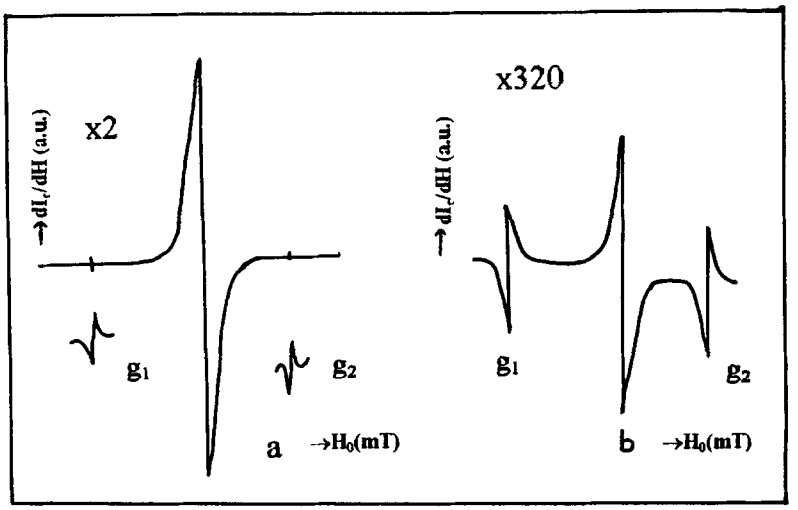

Figure 3. The ESR spectrum of nanometer-sized SnO_2 organosol at room temperature (microwave frequency: 9.3 GHz; microwave power: 1 mW; modulation frequency: 100 KHz; modulation amplitude: 2 Gauss; $g_1 = 1.981$; $g_2 = 2.034$) (a) sample 2; (b) sample 3.

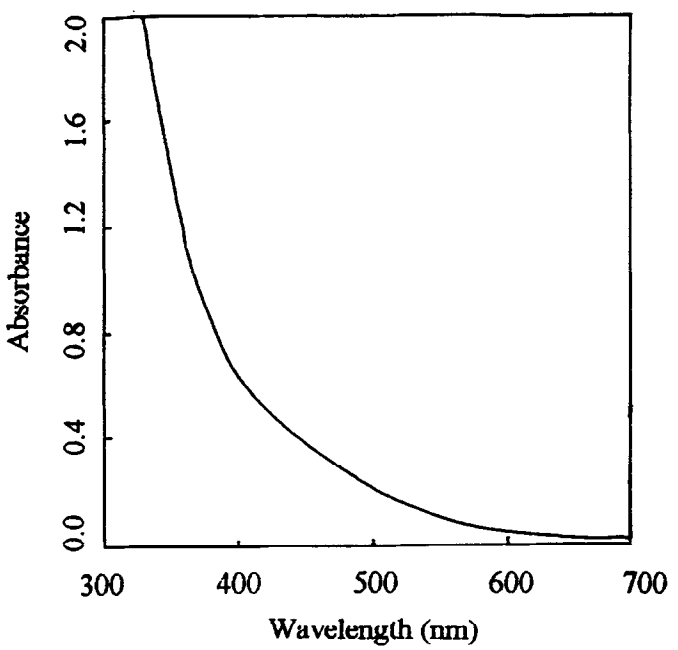

Figure 4. The absorption spectrum of nanometer-sized SnO_2 organosol.

The ESR results of sample 2 and sample 3 are shown in Figure 3a and b. The g-factors of both samples are the same and equal to 2.001 calculated by Mn^{2+} standard method. This g-factor is similar to that of paramagnetic center (F^+ center) formed by a free electron trapped in an oxygen

vacancy. The signal intensity of sample 2 is much stronger than that of sample 3 at the same sample amount. This difference indicates that the number of F^+-center-like oxygen vacancies in sample 2 is much larger than that in sample 3. From the analysis of the sample preparation process the amount of Sn^{4+} used in reaction is stoichiometrically larger than that of OH^- in order to ensure the prepared nanoparticles to have positive charges, which attract anionic surfactants to adsorb to the surface of nanoparticles to form stable nanoparticles. Therefore, there exist a lot of oxygen vacancies on the interface of sample 2, which can be stabilized by capped surfactants through the interaction between them. After high temperature treatment in air, the surfactant layer is burned off; and the nanometer-sized SnO_2 continues to oxidize, grow, and become more crystalline. High temperature treatment in sufficient oxygen largely reduces the number of oxygen vacancies and defect states. Therefore, the magnitude of ESR signal in sample 3 is reduced.

From the above analysis it may be concluded that there are a lot of oxygen vacancies on the interface of as-prepared nanoparticles, which entrap electrons to form the observed paramagnetic signals.

3.2 Absorption and Luminescence Spectra

Figure 4 presents the absorption spectrum of sample 1. It can be seen that when the wavelength is longer than 350 nm (band gap in bulk), the sample still has strong absorption. The absorption coefficient of an amorphous semiconductor can be written as (9)

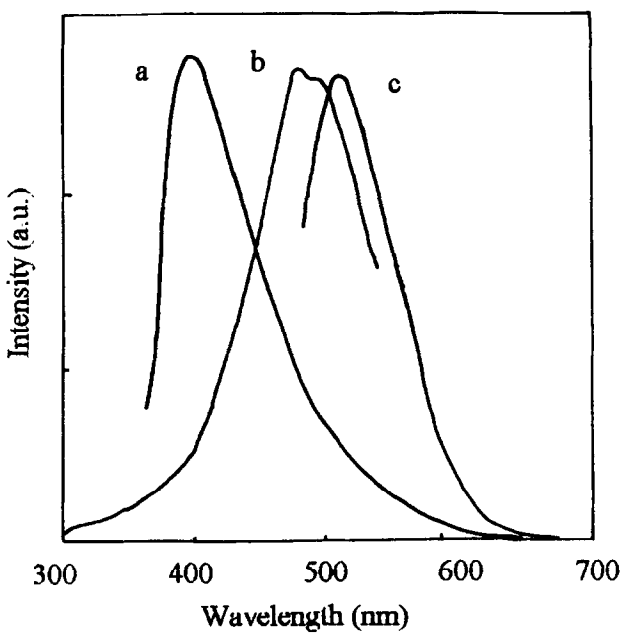

Figure 5. The excitation and photoluminescence spectra of nanometer-sized SnO_2 organosol: (a) the fluorescence spectrum of $\lambda ex = 330$ nm, $\lambda em,max = 390$ nm; (b) the excitation spectrum of $\lambda em = 540$ nm; (c) the fluorescence spectrum of $\lambda ex = 470$ nm, $\lambda em,max = 520$ nm.

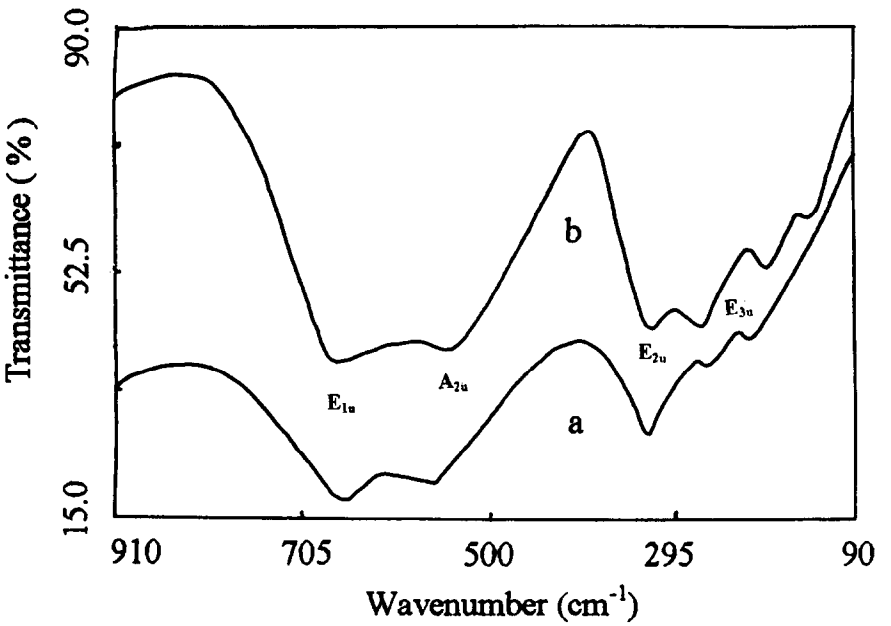

Figure 6. The IR transmittance spectra of nanometer-sized SnO_2. IR active TO modes frequency: A_{2u}:512; E_{1u}: 651; E_{2u}:297; E_{3u}:236 cm^{-1}. (a) sample 2, (b) sample 3.

$$\alpha h\omega = A(h\omega - Eg)^2 \qquad [1]$$

where α, $h\omega$, Eg are absorption coefficient, photon energy, and apparent optical bandgap, respectively. A is a constant characteristic of the amorphous semiconductor.

From formula [1] it can be seen that $(\alpha h\omega)^{1/2}$ has a linear relation with $h\omega$. The slope of the straight line gives Eg of material. The Eg of the prepared sample 1 is 2.25 eV, which red-shifts 1.45 eV compared with that of bulk SnO_2 (10). This is contrary to the quantum size effect which leads to the blue-shift of Eg with decrease of particle size, which has been observed in many nanometer-sized semiconductor materials (11). The red-shift of apparent optical band-edge of the prepared sample may come from the following two reasons. First, since the size of the sample is larger than the exciton Bohr radius of bulk SnO_2, 10 Å (12), the sample has a weak quantum confinement and the blue-shift of absorption band-gap due to the quantum size effect is very small. Second, the above ESR and XRD analyses have indicated that there are many oxygen vacancies due to nonstoichiometric ratio of reactants. These oxygen vacancies which mainly locate on the interface of nanoparticles have interactions with interfacial capping surfactants as shown in Figure 2b, and anionic surfactants as electron donors will stabilize F^+-center-like oxygen vacancies with positive charge. These interactions between interfacial oxygen vacancies and capped surfactants will lead to the formation of trapped states, which form a series of metastable energy levels within the band-gap, and result in the red-shift of apparent optical band-gap.

SnO_2 in bulk has no luminescence at room temperature (12), while the prepared sample 1 shows obvious photoluminescence at room temperature, as shown in Figure 5a, and c. Figure 5b is the excitation spectrum of λem = 520 nm, which exhibits a wide band excitation at wavelength

range from 350 to 500 nm, coinciding with the absorption band of the trapped state. This implies that the absorption of the trapped state contributes to the observed emission. These energy levels of trapped state are a series of metastable energy levels with relatively long lifetimes and their optical transitions are dipole allowed; therefore, the photoluminescence from this trapped state can be observed at room temperature.

From absorption and luminescence spectra, it can be concluded that the formation of trapped state, due to the interaction between interfacial oxygen vacancies and capped anionic surfactants, leads to the red-shift of absorption band-edge and photoluminescence at room temperature due to their relatively long lifetimes.

3.3 IR Absorption Spectra

Figures 6a and 6b are IR absorption spectra of samples 2 and 3, respectively. It is found that the whole IR spectral features of the two samples are similar, while there is an IR background absorption band in sample 2. Due to the strong background absorption band, the vibrational intensities, frequencies, and bandwidths of various vibrational modes in sample 2 accordingly change, as compared with those in sample 3. Detailed analyses of IR spectra have been published elsewhere (13). As discussed above, there exist many more trapped states with positive charges in sample 2 than in sample 3. This corresponds to accumulating relatively high surface charge density on the interface of sample 2. According to theoretical calculation (14), high surface charge density can lead to continuous absorption band within the IR transmittance spectrum.

3.4 Z-scan Study

The Z-scan curves of the sample excited with pulse laser are shown in Figure 7 a,b. From the Z-scan curve of sample 1, with closed-aperture arrangement, as shown in Figure 7a, it can be concluded that the sample belongs to defocusing materials and exists multiphoton absorption as discussed in the experimental section. Figure 7b further justifies the existence of multiphoton absorption with open-aperture arrangement. The ratio of two curves gives pure refractive nonlinearity. The nonlinear susceptibilities of the organic solvent and capping surfactant are smaller than 10^{-13} esu and can be neglected. Through calculation, the pure nonlinear refractive coefficient n_2 of sample 1 is - 2.8 x 10^{-10} esu, which is two-orders of magnitude larger than that of bulk SnO_2, 3.2 x 10^{-12} esu (5). The excitation of sample at 1.06 μm belongs to nonresonant excitation because the sample has no absorption at this wavelength. Therefore, the nonlinearities of thermalized refractive change and exciton effect due to linear absorption can be neglected. The origin of optical nonlinearity is mainly the electronic kerr effect. The enhancement of n_2 mainly comes from the quantum size effect and local field effect by interfacial capping surfactants, as discussed by other authors (15,16). Due to the relatively weak light intensity in our experiment (I_0 = 0.727 GW/cm^2), the absorption of free carrier induced by multiphoton absorption can be neglected, therefore the nonlinear absorption mainly comes from the multiphoton absorption. From the absorption spectrum we know that the band-gap of sample located at 540 nm, which is just longer than the wavelength of double frequency of 1.06 μm laser and satisfies the condition of two-photon absorption, $Eg < h\omega < 2Eg$. The two-photon absorption coefficient β, which was obtained through open-aperture arrangement, is 0.27 cm/GW.

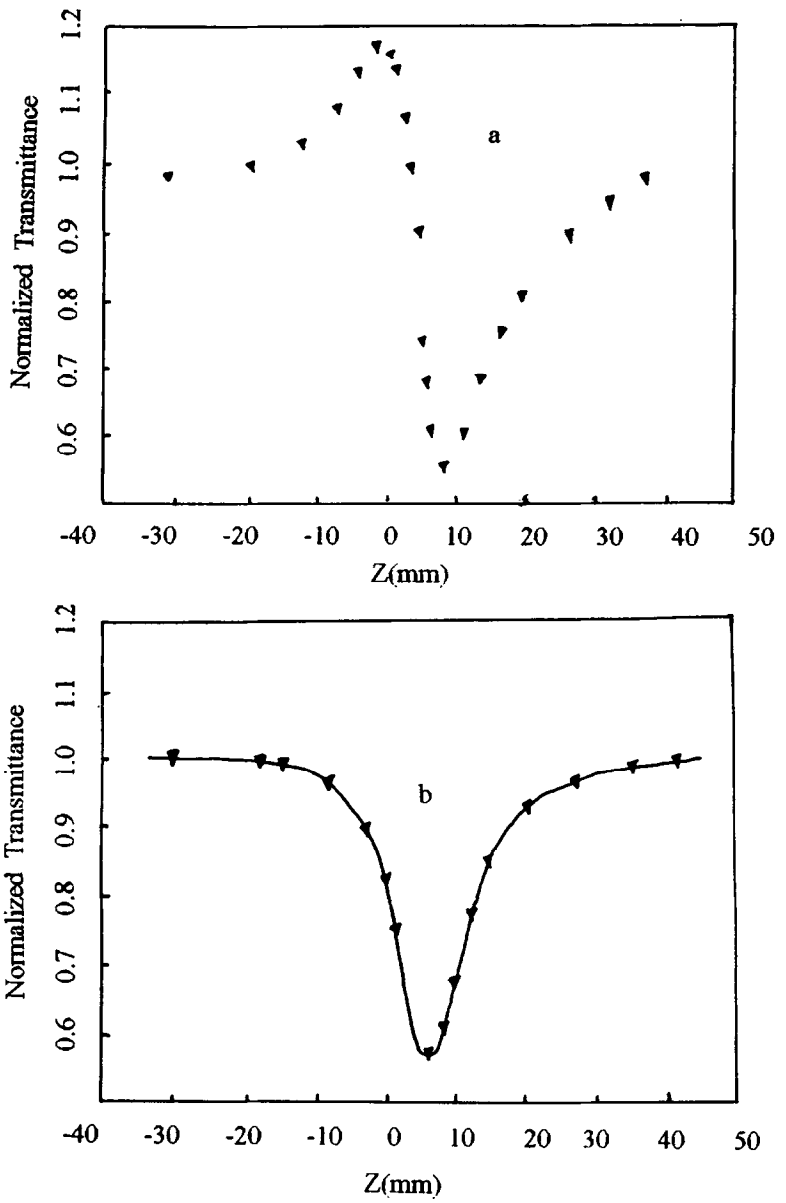

Figure 7. Z-scan normalized transmittance of nanometer-sized SnO_2 organosol excited by Q-switched Nd:YAG laser with a peak irradiance I_0 of 0.727 GW/cm^2: (a) closed-aperture (S = 0.34); (b) open-aperture (S = 1).

The Z-scan measurements of sample I excited with a cw Ar^+ laser indicate that the refractive nonlinearity also belongs to defocusing nonlinearity, while the absorptive nonlinearity belongs to

saturation absorption. The n_2 of sample 1 at 514.5 nm is -6.6 x 10^{-5} esu. The saturation absorption light intensity I_{sat} is lower than 10 W/cm^2. The excitation of sample with a cw Ar^+ laser at 514.5 nm belongs to resonant excitation because excitation wavelength is shorter than band-edge wavelength. From the linear absorption spectrum, on the one hand, it is known that the excitation of the prepared sample at λ = 514.5 nm comes from trapped state on the interface of nanoparticles, which shows strong electron-lattice interaction due to its strong interaction with capped surfactants and disorder of interfacial structure (17,18). The strong electron-lattice interaction indicates that the system has high nonirradiative efficiency, which can lead to large thermalized refractive nonlinearity at strong laser irradiation. Therefore, the large n_2 of the sample at 514.5 nm comes from thermalized refractive change. On the other hand, those trapped states exist in the form of metastable states, which have relatively long lifetimes. Their excitation under strong laser irradiation can lead to the nonlinear saturation absorption. The low saturation intensity of the sample is due to the long lifetimes and relatively high absorption coefficient of those trapped states.

4. CONCLUSIONS

From the above experiments and discussion, it can be seen that the prepared nanometer-sized SnO_2 organosol exhibits a series of new linear and nonlinear optical properties due to its special structural features. They can be summarized as follows: (i) Through XRD, it can be concluded that the as-prepared nanometer-sized SnO_2 sample mainly exists in the form of amorphous state and has interaction with capped surfactants. (ii) The existence of F^+-center-like oxygen vacancies is justified through ESR spectrum. (iii) The nanometer-sized SnO_2 organosol shows red-shift of absorption band-edge due to the formation of metastable energy levels of capped states within the prohibited band. These metastable energy levels can fluoresce at room temperature due to their relatively long lifetimes. (iv) IR spectrum is indicative of a high surface charge density. (v) From the pulse laser Z-scan study at the wavelength of 1.06 μm, n_2 of the sample is -2.8 x 10^{-10} esu, larger than that of the bulk. Due to the red-shift of band-gap, the two-photon absorption is also observed and β is 0.27 cm/GW. (vi) From the cw laser Z-scan study at the wavelength of 514.5 nm, the n_2 of the sample is -6.6 x 10^{-5} esu and belongs to thermally induced refractive nonlinearity. Due to the excitation of metastable energy levels of long life-time at this wavelength, low saturation absorption intensity is observed and the saturation light intensity I_{sat} is lower than 10 W/cm^2.

These new optical properties can be reasonably explained by its special interfacial structures under nanometer-sized range. These new optical properties also enlarge the applications of SnO_2 in nonlinear optics, such as optical switching and optical limiting.

ACKNOWLEDGMENT

The authors acknowledge the National Natural Science Foundation of China for financial support.

REFERENCES

1. Henglein, A., *Chemical Review*, 1989, 89, 1861.
2. Wang, Y., and Herron, N., *Journal of Physical Chemistry*, 1987, 91, 5005.
3. Jain, K.R., and Lind, R.C., *Journal of Optical Society of America*, 1983, 73, 647.

4. Yoffe, D.A., *Advanced Physics*, 1993, 42, 173.
5. Nie, W.J., *Advanced Materials*, 1993, 5, 520.
6. Mansor, S.B., Said, A.A., VanStryland, W.E., *Optical Letters*, 1989, 14, 955.
7. Mansor, S.B., Said, A.A., VanStryland, W.E., *IEEE Journal of Quantum Electronics*, 1990, 26, 760.
8. Zhang, D.Y., Wang, D. Zh., Wang, G.M., Wang, Zh., and Wu, Y.H., *Acta Physica Sinica*, 1991, 40, 844.
9. Mill, G., Li, Z.G., and Meisel, D., *Journal of Physical Chemistry*, 1988, 92, 822.
10. Arlinghaus, F.J., *Journal Physical Chemistry of Solids, 1974, 35, 931.*
11. Brus, L.E., *Applied Physics A*, 1991, 53, 465.
12. DeMurcia, M., Egee, M., Fillard, J.P., *Journal Physical Chemistry of Solids*, 1977, 39, 629.
13. Wu, X.C., Tang, G.Q., Zhang, G.L., et al., *Acta Optica Sinica*, 1995, 15, 1355.
14. Knipp, P.A., Reinecke, T.L., *Physics Review B*, 1992, 46, 10310.
15. Schmitt-Rink, S., Miller, D.A.B., Chemla, S.D., *Physics Review B*, 1987, 35, 8113.
16. Wang, Y., *Acc. Chem. Research*, 1991, 24, 133.
17. Galperin, Yu.M., Karpov, V.G., and Kozub, V.I., *Advanced Physics*, 1989, 38, 669.
18. Pnevmatikos, St., Yanovitskii, O., Friggis, Th, and Economou, E.N., *Physics Review Letters*, 1992, 68, 2370.